

# **Impact of Tip-Vortex Modeling Uncertainty on Helicopter Rotor Blade-Vortex Interaction Noise Prediction**

Stavros Vouros, Ioannis Goulos, Calum Scullion, Devaiah Nalianda and  
Vassilios Pachidis

*Centre for Propulsion Engineering*

*School of Aerospace Transport and Manufacturing*

*Cranfield University, Bedfordshire, MK43 0AL, UK*

## **Abstract**

Free-wake models are routinely used in aeroacoustic analysis of helicopter rotors; however, their semi-empiricism is accompanied with uncertainty related to the modeling of physical wake parameters. In some cases, analysts have to resort to empirical adaption of these parameters based on previous experimental evidence. This paper investigates the impact of inherent uncertainty in wake aerodynamic modeling on the robustness of helicopter rotor aeroacoustic analysis. A free-wake aeroelastic rotor model is employed to predict high-resolution unsteady airloads, including blade-vortex interactions. A rotor aeroacoustics model, based on integral solutions of the Ffowcs Williams-Hawkings equation, is utilized to calculate aerodynamic noise in the time-domain. The individual analytical models are incorporated into an uncertainty analysis numerical procedure, implemented through non-intrusive Polynomial Chaos expansion. The potential sources of uncertainty in wake tip-vortex core growth

Presented at the 45<sup>th</sup> European Rotorcraft Forum, Warsaw, Poland, September 17-20, 2019

*Corresponding and lead author at; Centre for Propulsion Engineering, School of Aerospace, Transport and Manufacturing, Cranfield University, Building 52, Room G54, Bedfordshire, MK43 0AL, UK, Tel.: +44 (0) 1234 75 8286, e-mail address: vourosstavros@windowlive.com (S. Vouros)*

modeling are identified and their impact on noise predictions is systematically quantified. When experimental data to adjust the tip-vortex core model are not available the uncertainty in acoustic pressure and noise impact at observers dominated by blade-vortex interaction noise can reach up to 25% and 3.50 dB respectively. A set of generalized uncertainty maps is derived, for use as modeling guidelines for aeroacoustic analysis in the absence of the robust evidence necessary for calibration of semi-empirical vortex core models.

**Keywords:** Computational aeroacoustics, Free-wake aerodynamics, Helicopter noise prediction, Uncertainty quantification, Blade-vortex interaction noise.

### Nomenclature

#### *Roman Symbols*

$A_{cs}$	Blade element cross sectional area	$m^2$
$a_i, i = 0, 1, \dots, p$	Coefficient of orthogonal polynomial basis function	-
$c_0$	Speed of sound	m/s
$c_b$	Blade chord	m
$C_L$	Rotor disc rolling moment coefficient = $L / (\rho \pi \Omega^2 R^5)$	-
$C_M$	Rotor disc pitching coefficient = $M / (\rho \pi \Omega^2 R^5)$	-
$C_n M^2$	Blade element normal force coefficient = $F_n / (0.5 \rho c_0^2 c_b)$	-
$C_T$	Rotor disc thrust coefficient = $T / (\rho \pi \Omega^2 R^4)$	-
$COV$	Coefficient of variation = $\mu / \sigma$	-
$d$	Normal distance between a point and a vortex filament	m
$dy$	Blade differential span length	m

$f = 0$	Acoustic data line function	-
$F_n$	Sectional normal force	N/m
$\vec{l}_{12}$	Vortex filament vector	m
$\vec{L}$	Blade sectional loading vector	N/m
$L$	Rotor rolling moment	Nm
$\vec{M}$	Relative Mach number vector	-
$ \vec{M} $	Magnitude of relative Mach number	-
$M$	Rotor pitching moment	Nm
$Mo$	Mode (value with highest probability) of distribution	unit
$n$	Number of uncertain input parameters	-
$N_{Pearson}$	Pearson's correlation index	-
$OASPL$	Overall Sound Pressure Level	dB
$p$	Order of polynomial expansion	-
$p'$	Acoustic pressure	Pa
$p'_m$	Monopole acoustic pressure	Pa
$p'_d$	Dipole acoustic pressure	Pa
$\vec{r}$	Position vector of a point on a vortex filament	m
$\hat{r}$	Unit radiation vector	-
$r$	Radiation distance	m
$r_c$	Tip vortex viscous core radius	m
$r_{c0}$	Initial tip vortex viscous core radius	m
$\vec{r}_1$	Position vector of a point relative to the beginning of a vortex filament	m
$\vec{r}_2$	Position vector of a point relative to the end of a vortex	m

	filament	
$R$	Rotor radius	m
$R(n,m)$	Shorthand notation function	$m^{-n}$
$S_i$	Sobol sensitivity index	-
$t$	Observer time	s
$T$	Rotor thrust	N
$\vec{V}_{ind}$	Induced velocity vector	m/s
$W$	Shorthand notation term	m/s
$\vec{x}$	Observer position vector, with components $x_i$	m
$y$	Non-deterministic response of system at a collocation point	unit
$\gamma$	Non-deterministic response of system	unit

***Greek Symbols***

$\alpha$	Oseen constant for the vortex core radius	-
$\alpha_1$	Squire parameter for the eddy viscosity factor	-
$\alpha_s$	Wind tunnel rotor shaft angle	rad
$\Gamma$	Circulation	$m^2/s$
$\gamma_1$	Skewness of distribution	-
$\gamma_2$	Kurtosis of distribution	-
$\Delta\gamma_2$	Excess Kurtosis relative to Gaussian = $\gamma_2 - \gamma_2^{Gaussian}$	-
$\delta$	Eddy viscosity parameter	-
$\varepsilon$	Actual fractional error	unit
$\zeta$	Distance along trailed tip vortex	rad
$\mu$	Mean value of distribution	unit
$\nu$	Kinematic viscosity	$m^2/s$

$\xi$	Distribution	-
$\rho_0$	Density of quiescent medium	kg/m <sup>3</sup>
$\sigma$	Standard deviation of distribution	unit
$\varphi_i, i = 0, 1, \dots, p$	Polynomial basis function	-
$\psi$	Blade azimuthal position	rad
$\Omega$	Rotor rotational speed	rad/s

***Subscripts***

$(\cdot)_{amp}$	Amplitude
$(\cdot)_0$	Property referring to the quiescent acoustic medium

***Superscripts***

$(\cdot)^{adv}$	Quantity referring to rotor advancing side
$(\cdot)^{exact}$	Theoretically exact value of acoustic quantity
$(\cdot)^{inflow}$	Vortex core quantity used to evaluate induced velocity for inflow calculations
$(\cdot)^{ret}$	Quantity referring to rotor retreating side
$(\cdot)^{wake}$	Vortex core quantity used to evaluate induced velocity for wake calculations

**Introduction**

Helicopter noise prediction is affiliated with the aerodynamic modeling of the rotor flowfield (Ref. 1). Free-wake aerodynamic modeling methods are capable of efficiently predicting complex aerodynamic phenomena like blade-vortex interactions (BVI), through detailed resolution of rotor wake behavior (Ref. 2). The aforementioned models require some user-defined input parameters related to rotor

wake physics, in particular, related to the modeling of the viscous tip-vortex core. These parameters are typically obtained from experiments or empiricism; hence they are associated with inherent uncertainty which is propagated in the prediction of rotor wake geometry, wake-induced inflow, aerodynamic loads and consequently, aeroacoustic behavior. The identification of wake aerodynamic sources of uncertainty and quantification of their impact on aeroacoustic predictions are essential towards the design, certification and operation of present and future rotorcraft.

The majority of aeroacoustic uncertainty investigations to date have been focused on geometrical and operational input uncertainties. In Ref. 3 a benchmark rod-airfoil configuration was assessed in terms of geometric uncertainty and its propagation in aeroacoustics. A Large-Eddy Simulation (LES) solver was coupled with an aeroacoustic solver within a non-intrusive stochastic collocation method (Ref. 4). It was shown that an uncertainty of  $\pm 40\%$  in the position of the rod relative to its diameter led to an uncertainty of 0.5-1 dB in the Overall Sound Pressure Levels (OASPL) (Ref. 3).

Olsman (Ref. 5) quantified the uncertainty associated with ground acoustic footprint of noise abatement flight procedures in the presence of randomness in the operational flight path. A noise hemisphere approach was employed for the prediction of noise footprint and incorporated into an uncertainty quantification method based on Polynomial Chaos expansion (PCE). Standard deviations of up to 3 dB were calculated with respect to the deterministic solution, which highlight the importance of a non-deterministic approach in the prediction of helicopter ground noise impact.

Ricks *et al.* (Refs. 6,7) explored the impact of operational and geometrical uncertainty in the noise propagation stage of hybrid computational aeroacoustics. A Computational Fluid Dynamics (CFD) solver based on the inviscid Euler equations

was coupled with an integral solution of the Ffowcs Williams-Hawkings (FW-H) equation for the prediction of noise propagation. A non-lifting helicopter rotor in hover was considered and an in-plane noise observer located 3.09 radii upstream of the rotor. PCE was employed for the quantification of uncertainty and sensitivity analysis using Sobol indices. Uncertainty of 7.36% was observed in the peak acoustic pressure attributed to the randomness in blade tip Mach number. The investigations were carried out for in-plane observers dominated by thickness noise.

Gennaretti *et al.* (Ref. 2) assessed the capabilities of a boundary element methodology as regards BVI noise prediction. The study included a sensitivity analysis which showed that the wake model is sensitive to variations of initial vortex core radius and growth rate. The analysis was a sensitivity investigation, based on the assumption of  $\pm 50\%$  variation of wake diffusion parameters.

Bhagwat and Ramasamy (Ref. 8) examined the effect of tip-vortex aperiodicity on the measurement uncertainty of vortex-core properties, accrued through particle image velocimetry (PIV). As depicted by Mula *et al.* (Ref. 9) and van der Wall and Richard (Ref. 10), adequate seeding of the tip vortex core constitutes a major challenge of PIV measurements. This is due to the impact of centrifugal forces acting on heavier particles, which yield lower levels of light scattered by the lighter particles (Ref. 11). Uncertainties in the order of 10% were calculated for the vortex core radius of the HART II rotor (Ref. 12) in BVI conditions. The aforementioned levels of uncertainty are comparable with uncertainty levels present in state-of-the-art in tip-vortex measurements; however they have never been incorporated into helicopter rotor aeroacoustic simulation. In some cases, robust experimental evidence referring to tip-vortex core radius is not available, forcing analysts to resort to empiricism for the determination of the associated physical properties necessary for

aerodynamic calculations.

The vortex core radius is a critical aerodynamic parameter which affects airloads and consequently, noise. To the authors' knowledge, the impact of tip-vortex core modeling uncertainty on the robustness of aeroacoustic predictions has not been systematically investigated in the published literature. The scope of this work is the quantification of the impact of wake modeling uncertainty on helicopter rotor BVI noise predictions. Furthermore, it is aimed to devise a set of modeling guidelines applicable when uncertainty is present in the tip-vortex core physical parameters.

### **Mathematical formulation**

A mathematical formulation is deployed for modeling helicopter rotor noise under uncertainty. A free-wake aeroelastic rotor model is used to predict unsteady rotor airloads including blade-vortex interactions. A set of integral solutions of the FW-H equation is employed for modeling helicopter rotor aeroacoustic behavior. Finally, a point collocation method is utilized to investigate the impact of tip-vortex core growth modeling uncertainty on the aeroacoustic analysis of helicopter rotors.

### **Aeroelastic rotor model**

A free-wake and unsteady aeroelastic rotor model is utilized to predict elastic rotor blade unsteady motion and unsteady airloads, including BVIs (Ref. 13). A minimum potential energy method, similar to the one reported in Ref. 14, is deployed for the estimation of coupled flap-lag-torsion vibration characteristics of the elastic rotor blades (Ref. 15). The matrix/vector based formulation presented in Ref. 16 is employed for modeling the flexible rotor blade kinematics along with the Leishman-Beddoes indicial response method (Ref. 17) for the prediction of unsteady blade



airloads. The aforementioned models have been extensively described in the corresponding references; thus, further discussion will be omitted.

A relaxation-type free-wake aerodynamic model is employed to model the unsteady and periodic wake-induced inflow on the rotor disc, therefore enabling the identification of complex BVI phenomena (Ref. 18). Each vortex is discretized as a series of straight vortex filaments with Lagrangian markers located at the ends of each filament. It is assumed that viscous effects are significant only within the vortex core region of each vortex filament. Subsequently, the flow can be considered as inviscid outside the vortex singularity (Ref. 19). The governing equation which describes the convection of the Lagrangian markers is the unsteady Vorticity Transport Equation for incompressible and isotropic fluids (Ref. 19).

The velocity induced by a single vortex filament is evaluated through numerical integration using the Biot-Savart law for straight vortex filaments including the Vatistas vortex core model (Ref. 20):

$$\vec{V}_{ind} = \frac{\Gamma}{4\pi} \left( \frac{d}{(r_c^{2n} + d^{2n})^{1/n}} \right) \frac{\vec{l}_{12}}{|\vec{l}_{12}|} \cdot \left( \frac{\vec{r}_1}{|\vec{r}_1|} - \frac{\vec{r}_2}{|\vec{r}_2|} \right) \cdot \left( \frac{\vec{l}_{12} \times \vec{r}}{|\vec{l}_{12} \times \vec{r}_1|} \right) \quad (1)$$

where  $\Gamma$  is the circulation strength of the vortex filament,  $\vec{l}_{12}$  is the vortex filament vector,  $\vec{r}_1$  and  $\vec{r}_2$  are the position vectors of the arbitrary point P relative to the Lagrangian markers of the filament and  $\vec{r}$  is the position vector of point P relative to the vortex segment, as shown in Fig. 1. The normal distance between point P and the vortex filament is  $d = |\vec{l}_{12} \times \vec{r}| / |\vec{l}_{12}|$ . The tangential velocity profile of the Vatistas model is defined by the general constant  $n$  which best matches the experimental velocities measured in Ref. 20. Finally, the vortex core radius  $r_c$  is given by Squire's equation:

$$r_c(\zeta) = \sqrt{r_{c0}^2 + 4\alpha\delta\nu\frac{\zeta}{\Omega}} \quad (2)$$

where  $r_{c0}$  is the initial core radius,  $\alpha = 1.25643$  is the Oseen constant,  $\zeta$  is the filament age and  $\Omega$  is the rotational speed. The eddy viscosity factor  $\delta$  is :

$$\delta = 1 + \alpha_1 \frac{\Gamma}{\nu} \quad (3)$$

Bhagwat *et al.* (Ref. 21) suggested values in the order of  $10^{-4}$  to  $10^{-3}$  for the Squire parameter  $\alpha_1$  to represent viscous core growth of small scale rotors. Although initial vortex core radii of 5-10% chord are usually used for forward flight, a larger initial core radius  $r_{c0} = 0.6c$  has been used in some studies to reduce spurious BVI response in descending flight (Ref. 12). Different core radii may be used for the evaluation of induced velocity for wake calculations and rotor inflow calculations, to improve convergence stability and speed (Ref. 12). From a physical perspective, the use of different core radii is attributed to discrepancies between the aerodynamic environment of the rotor and the wake, specifically: (a) difference in blockage effects due to blade solidity and due to fuselage geometry, and (b) difference in turbulence levels upstream and downstream of the rotor disc.

Both  $r_{c0}$  and  $\alpha_1$  affect the radius of the tip vortex core, which acts as “damper” in the calculation of induced velocity. Higher values of these two parameters lead to lower induced velocity magnitudes; hence lower magnitude of aerodynamic forces. For the present analysis, the values of  $r_{c0}^{wake} = 0.1c$  and  $\alpha_1^{wake} = 0.001$  are used for wake calculations, and  $r_{c0}^{inflow} = 0.6c$  and  $\alpha_1^{inflow} = 0.008$  for rotor inflow calculations. These values provide the best match between predicted and measured noise data for the HART-II rotor baseline case. The aforementioned set of tip vortex growth parameters will serve as mean values for the uncertainty analysis

and will be coupled with appropriately chosen statistical distributions around them.

The wake is split in the near wake and far wake regions which are linked via a vortex roll-up model based on the distribution of bound circulation and local vorticity  $\partial\Gamma(r)/\partial r$ . Shed vortices are not resolved in the wake model as they are accounted for in the unsteady blade aerodynamic model through the deficiency functions applied on the circulatory normal force coefficient (Ref. 17).

The individual models are integrated into a globally-convergent trim algorithm based on Broyden's numerical algorithm. The trim algorithm solves for the rotor collective and longitudinal and lateral cyclic controls for given wind tunnel operating conditions and rotor thrust  $C_T$ , rolling  $C_L$  and pitching moment  $C_M$  coefficients.

### **Rotor aeroacoustics model**

The noise prediction code ICARUS (Integral Computational AeRoacoustics Unified Software), is deployed to model helicopter rotor aeroacoustics (Ref. 22, 23). This code is an integral implementation of the Ffowcs Williams-Hawkings (FW-H) equation (Ref. 24), which is the most general form of Lighthill's Acoustic Analogy (Ref. 25). The FW-H equation describes acoustic pressure disturbances as a three-dimensional wave, induced by monopole, dipole and quadrupole noise sources.

Formulation 1A of Farassat (Ref. 26, 27) is the most frequently used and extensively validated integral solution of the FW-H equation. It is based on the free-space Green's function solution of the three-dimensional wave equation. Formulation 1A resolves thickness and loading noise components, which can be described by monopole and dipole acoustic terms, respectively. The high-speed impulsive noise component which corresponds to the quadrupole term of the FW-H equation is neglected. This assumption is valid as long as the rotor tip Mach number is below the

transonic limit, which is the typical condition for the majority of flight cases dominated by BVI noise which is the focus of this work.

Chordwise compact acoustic expressions of Formulation 1A are utilized since the blade chord can be considered small compared to the wavelength of the radiated acoustic content (Ref. 19). Brentner *et al.* (Ref. 28) introduced a compact form of the loading noise term of the Formulation 1A, utilizing the blade-element lift distribution  $\bar{L}$  across the blade span. Consequently, the computation reduced from a surface integral to a line integral. Lopes (Ref. 29) presented and validated a compact expression of the monopole term of Formulation 1A, based on the chordwise compactness assumption which dictates that the radiation distance is large compared to the blade chord. The proposed formulation utilizes the spanwise distribution of the airfoil cross-sectional area  $A_{cs}(y)$  as a blade design parameter of each blade element with differential span length  $dy$ . Hence, the acoustic pressure due to thickness effects is also evaluated as a line integral defined by the line equation  $f=0$ . Using the shorthand notation introduced by Lee *et al.* (Ref. 30) and followed by Lopes (Ref. 29), the compact expressions of thickness and loading acoustic pressure employed in this work can be formed as follows:

$$\begin{aligned} \frac{4\pi}{\rho_0} p'_m(\vec{x}, t) = & \int_{f=0} A_{cs} \left( W + \frac{\partial W}{\partial \tau} \right) R(2, 4) \Big|_{ret} dy \\ & + \int_{f=0} 2A_{cs} W^2 R(3, 5) \Big|_{ret} dy \\ & - \int_{f=0} c_0 A_{cs} \frac{\partial \vec{M}}{\partial \tau} \cdot \hat{r} R(2, 3) \Big|_{ret} dy \end{aligned} \quad (4)$$

$$\begin{aligned}
4\pi c_0 p'_d(\vec{x}, t) = & \int_{f=0} \frac{\partial \vec{L}}{\partial \tau} \cdot \hat{r} R(1, 2) \Big|_{ret} dy \\
& + \int_{f=0} c_0 \left( \vec{L} \cdot \hat{r} - \vec{L} \cdot \vec{M} \right) R(2, 2) \Big|_{ret} dy \\
& + \int_{f=0} \vec{L} \cdot \hat{r} W R(2, 3) \Big|_{ret} dy
\end{aligned} \tag{5}$$

where  $p'_m$  and  $p'_d$  are the monopole and dipole acoustic disturbance terms respectively, evaluated at the observer position  $\vec{x}$  and observer time  $t$  and  $c_0$  and  $\rho_0$  are the speed of sound and density of the quiescent acoustic medium, respectively. The vectors  $\vec{L}$ ,  $\vec{M}$  and  $\hat{r}$  correspond to the aerodynamic loading vector, the local relative Mach number vector and the unit radiation vector, respectively. It is noted that the time derivatives are being evaluated in the source time  $\tau$ . The subscript "ret" represents numerical integration within the retarded-time (i.e. source-time). The following shorthand functions are being used, as suggested by Lopes (Ref. 29):

$$R(n, m) = r^{-n} \left( 1 - \vec{M} \cdot \hat{r} \right)^{-m} \tag{6}$$

$$W = r \frac{\partial \vec{M}}{\partial \tau} \cdot \hat{r} + c_0 \left( \vec{M} \cdot \hat{r} - |\vec{M}|^2 \right) \tag{7}$$

The source-time-derivative of the function  $W$  has been analytically determined by Lee (Ref. 30):

$$\frac{\partial W}{\partial \tau} = r \frac{\partial^2 \vec{M}}{\partial \tau^2} \cdot \hat{r} - 3c_0 \frac{\partial \vec{M}}{\partial \tau} \cdot \vec{M} + \frac{c_0}{r} \left( r \frac{\partial \vec{M}}{\partial \tau} \cdot \hat{r} + c_0 \left( \left( \frac{\partial \vec{M}}{\partial \tau} \cdot \hat{r} \right)^2 - |\vec{M}|^2 \right) \right) \tag{8}$$

where  $r$  is the radiation distance and  $|\vec{M}|$  is the magnitude of the local relative Mach number vector.

The overall discrete frequency acoustic pressure  $p'(\vec{x}, t)$  can be expressed as the summation of monopole and dipole acoustic contributions. The compact acoustic formulations adopted in this study are compatible with the lifting-line-type aerodynamic input provided by the free-wake airloads model. Moreover,

computational savings of up to 99.5% have been reported with only slight deviations compared to the corresponding non-compact discrete-frequency acoustic pressure computations (Ref. 30, 31).

### Uncertainty quantification method

Traditional approaches for uncertainty analysis involve Monte Carlo (MC) simulation which is based on random sampling of the uncertain input parameters. Subsequently, deterministic evaluations of the investigated model are performed for each sample point and the output quantities of interest are statistically examined. MC methods are widely used due to ease of implementation, but the number of samples required for convergence of the statistical properties of the outputs is typically in the order of thousands of evaluations (Ref. 32, 33). This number becomes prohibitive when the deterministic model evaluations are computationally demanding.

Point collocation methods constitute an efficient alternative to computationally expensive MC methods for uncertainty quantification (UQ). PCE has been utilized for UQ in aeroacoustics (Refs. 5,7). A PCE approach (Ref. 34) is employed for the quantification of uncertainty in aeroacoustic analysis due to the uncertainty in wake initial tip vortex core radius and growth rate utilized in this work. PCE describes the response  $Y(\xi)$  of a system encompassing non-deterministic input of known distribution  $\xi$  as an infinite series of orthogonal polynomial basis functions, provided that the response behavior is smooth. For practical engineering applications, the infinite series is truncated to a number of  $p+1$  basis functions, where  $p$  is the order of the polynomial. Hence:

$$Y(\xi) = \sum_{i=0}^p \varphi_i(\xi) a_i \quad (9)$$

where  $a_i$ ,  $i=0,1,\dots,p$  are the coefficients of the orthogonal polynomial basis functions.

It is noted that the orthogonal polynomials basis functions  $\varphi_i(\xi)$ ,  $i=0,1,\dots,p$  are dependent only upon the type of the known random distribution  $\xi$ . Therefore, the estimation of the system's response, according to Eq. (9), requires only the determination of the coefficients  $a_i$ ,  $i=0,1,\dots,p$  of the polynomial terms. These are determined by solving the linear system of equations defined by the expansion of Eq. (9) into forming Eq. (10):

$$\begin{bmatrix} y(\xi_0) \\ \vdots \\ y(\xi_m) \end{bmatrix} = \begin{bmatrix} \varphi_p(\xi_0) & \cdots & \varphi_0(\xi_0) \\ \vdots & \ddots & \vdots \\ \varphi_p(\xi_m) & \cdots & \varphi_0(\xi_m) \end{bmatrix} \begin{bmatrix} a_p \\ \vdots \\ a_0 \end{bmatrix} \quad (10)$$

where  $\xi_i$ ,  $i=0,1,\dots,p$  are the  $m+1$  collocation points at which the system's deterministic response is evaluated,  $y(\xi_i)$  is the response of the system at each collocation point and  $a_i$  the unknown coefficients of the polynomial of order  $p$ . The number of collocation points required for the solution of the linear system of equations with  $n$  uncertain input parameters and orthogonal polynomials of order  $p$  is the cardinality of the dataset  $\Xi$  and is given by:

$$card(\Xi) = 1 + \sum_{i=1}^p \frac{1}{i!} \prod_{j=0}^{i-1} (n+j) = \frac{(n+p)!}{n!p!} \quad (11)$$

The low-discrepancy Halton sequence is employed for the determination of collocation points, which offers better coverage of the design space compared to random sampling methods (Ref. 35). Typically, over-sampling is required to improve the accuracy of the system's response approximation with PCE (Ref. 35). The polynomial expansion is finally derived through least-squares regression, based on the minimization of the error of the fitting function (Ref. 36).

For the purposes of this work the developed PCE-based approximation will be

used as a meta-model to be provided to a MC analysis method. The proposed PCE-MC method allows approximating and exploring the available hyperspace in terms of statistical properties. PCE treats the deterministic model as a black-box; hence the developed strategy is a non-intrusive method for uncertainty quantification, which is a suitable approach for engineering applications. Additionally, PCE enables the capability of directly performing variance-based sensitivity analysis to identify the relative sensitivity of the non-deterministic output to the uncertain input parameters. Sensitivity analysis based on Sobol indices  $S_i$  (Ref. 37, 38) is allowed when the response of the system can be decomposed in summands that are mutually orthogonal. An overview of the integrated statistical method is presented in Fig. 2.

## Results and discussion

### Comparison with experimental measurements

The accuracy of the developed simulation method is assessed through comparing predictions with experimental measurements retrieved from the baseline case of the HART II rotor (Ref. 12). The rotor is a 40% dynamically and Mach scaled model of the 4-bladed hingeless Bo 105 helicopter rotor. The rotor radius is  $R = 2 \text{ m}$  and the rotational speed is  $\Omega = 109.12 \text{ rad / s}$ . The rotor shaft is tilted backwards with a shaft angle  $\alpha_s = -4.5 \text{ deg}$ , advance ratio  $\mu = 0.15$  and thrust coefficient  $C_T = 0.0044$ .

Before conducting the comparisons with experiments, the numerical uncertainty associated with aeroacoustic modelling is assessed in terms of computational grid convergence investigations. the discretization error due to the following parameters is discussed: (a) rotor blade radial discretization, (b) rotor azimuthal discretization, (c) near-wake azimuthal discretization, (d) near-wake extent,



(e) far-wake extent. The computational grid is assessed in terms of the following two aeroacoustic descriptors: (a) amplitude of acoustic pressure  $p'_{amp}$  at the advancing-side ground observer of the HART-II experiment and (b)  $OASPL$  at the same observer located 2.215 m below the rotor disc, 0.0 m upstream and 1.81 m at the advancing side of the rotor.

Roache (Ref. 39) proposed a method which provides an objective asymptotic approach for the quantification of numerical uncertainty in grid convergence. The theoretically exact values of the acoustic objectives  $p'^{exact}_{amp}$  and  $OASPL^{exact}$  are estimated based on Richardson Extrapolation (Ref. 39). The exact values represent the solution that would theoretically occur after an infinitely fine numerical grid implementation. For this reason, the inverse values of number of radial blade elements, near wake extent and far wake extent have been preferred to match the zero value of the discretization step corresponding to the solution of the Richardson Extrapolation.

Grid convergence is assessed via quantifying the actual fractional error with respect to the theoretically exact solutions. Relative deviations are provided for acoustic pressure amplitude,  $\varepsilon_{p'_{amp}} = \frac{p'_{amp} - p'^{exact}_{amp}}{p'^{exact}_{amp}} [\%]$ , whilst dB differences are preferred for overall noise,  $\varepsilon_{OASPL} = OASPL - OASPL^{exact} [dB]$ . Fig. 3 (a) presents the relative deviations of  $p'_{amp}$  from  $p'^{exact}_{amp}$  for the five parameters under investigation, whilst Fig. 3 (b) presents the corresponding values for  $OASPL$ . Overall it is shown that a coarse discretization leads to under-prediction of noise. The gray markers represent the discretization parameters employed in this work, as well as the associated levels of numerical uncertainty. Specifically, rotor blades comprise 30

radial elements, resolving an 1 deg. rotor azimuthal step and 10 deg. near wake azimuthal step, whilst the near wake is truncated at 30 deg. and 3 far wake rotations are considered. It will be shown that the accrued levels of numerical uncertainty are at least one order of magnitude lower than the uncertainty levels calculated due to tip vortex input parameters.

Fig. 4 (a) presents a comparison of predicted and measured acoustic pressure history at the advancing side observer. It is shown that the developed method captures the behavior of the measured acoustic pressure signal. A spectral comparison of the acoustic pressure time histories is required to thoroughly quantify the predictive accuracy of the aeroacoustic formulation. Fig. 4 (b) presents the spectral content of the predicted acoustic signal, compared with the corresponding noise results of the measured acoustic history in the range between the 1<sup>st</sup> and 40<sup>th</sup> multiples of the Blade Passage Frequency (BPF), where low-harmonic and BVI noise dominate (Ref. 12). It is observed that the measured acoustic signal is not periodic due to the additional pressure sensors installed on Blade 1, which caused flapping and loading discrepancies relative to Blades 2-4 (Ref. 12). Due to the aperiodicity of the acoustic signal, each of the pulses of the measured signal have been individually analyzed. As regards the low-frequency content of the noise signal, good agreement between predictions and measurements is observed for the first five BPF harmonics, albeit with discrepancies associated with the 4<sup>th</sup> and 5<sup>th</sup> harmonic. These can be attributed to the deviations observed around the second negative peak of each acoustic pulse and especially in pulses 3 and 4. For the higher-frequency content, good agreement is observed up to the 30th harmonic, with an average deviation of 6.5dB, which is sufficient for capturing the primary effects associated with BVI phenomena.

Fig. 5 (a) illustrates the noise contour maps corresponding to the BL case of

the HART II experiment. The measurement plane is located 2.215 m below the rotor disc. The OASPL were calculated via frequency-integration of the Fast Fourier Transformation (FFT) on the original acoustic pressure signal at microphone location. Only BPF harmonics between the 6<sup>th</sup> and the 40<sup>th</sup> were considered to isolate the mid-frequency content of the emitted noise, where BVI noise is dominant. Fig. 5 (b) presents the predicted noise contour maps for the same conditions using the developed computational models. It can be seen that the advancing and retreating side BVI peaks are accurately predicted in terms of directivity and intensity. An average absolute deviation of 4.1 dB was calculated, which can be deemed as satisfactory given the complexity of the simulated case. It is noted that the experimental scatter of the noise radiation was found to be up to 2 dB (Ref. 12).

### Polynomial Chaos expansion

The flowfield in the viscous vortex core region is governed by shear-stress terms and rotational flow. The uncertain input parameters considered in this work are the governing parameters of the tip-vortex core radius model, namely,  $r_{c0}^{wake}$ ,  $\alpha_1^{wake}$ ,  $r_{c0}^{inflow}$  and  $\alpha_1^{inflow}$ . Two distinct cases of input uncertainty are examined: (a) the case when experimental data referring to tip vortex core geometry are available and (b) the case of absent experimental data. For the case of available experimental data, uncertainty is concentrated around the mean values associated with each parameter.

Various methods have been employed for the measurement and post-processing of PIV data referring to helicopter tip vortex core properties (Ref. 8–11). Bhagwat and Ramasamy (Ref. 8) discussed the uncertainty in PIV measurements of tip-vortex core radius and circulation strength. Their study included quantifications for the HART-II rotor, therefore these results will be used to keep consistency with

the rotor employed in the present paper. For the HART-II rotor, a  $COV=11.5\%$  was measured for core radius and  $COV=9.9\%$  for circulation. No evidence is available with respect to uncertainty in the selection of Squire parameter  $\alpha_1$ . As presented in Eq. (2), the eddy viscosity parameter  $\delta$  is in the square root of the tip vortex core equation. However, the analysis presented in this section will be extended to a fundamental study for different levels of uncertainty. Therefore a consistent  $COV$  value will be used for the all uncertain parameters, representative of the order of magnitude of the  $COV$  levels reported in Ref. 8. Consequently, the probability density function (PDF) of all input parameters will be considered to be Gaussian with coefficient of variation  $COV = 10\%$ . The associated values of mean  $\mu$  and standard deviation  $\sigma$  are summarized in Table 1.

As regards the case of absent experimental data for tip-vortex core radius calibration, a uniform distribution is used for all uncertain inputs, as they can take any value within the designated limits, with equal probability of occurrence. The determination of the upper and lower limit for each input is dependent upon the availability of relevant literature and practical experience. Based on the suggestions of Ref. 21 and Ref. 12, as well as the discussion in the “Mathematical formulation” section, an uncertainty of  $COV = 30\%$  will be adopted for this investigation, which can be considered as a relatively conservative choice. The resulting limits of the uniform distribution of each uncertain input variable are also provided in Table 1.

The design space is discretized based on the sampling method described in the “Mathematical formulation” section. An over-sampling coefficient of 4 is used in this work to generate a reliable sample. A polynomial order  $p = 2$  is selected in this work, as also followed in Ref. 7. Based on Eq. (11) and for the given number of uncertain inputs  $n = 4$ , a total of 60 collocation points occur for the PCE. The coupled approach

comprising free-wake aerodynamics and ICARUS aeroacoustics is employed for the evaluation of each collocation point, as shown in Fig. 2. The output objectives of interest constitute aerodynamic and aeroacoustic descriptors of parameters which govern BVI noise generation and propagation. Specifically, the objectives chosen for UQ are: (a) amplitude of time-derivative of normal force coefficient at  $0.87R$  on the advancing side of the rotor  $\left(dC_n M^2/d\psi\right)_{amp}^{adv}$ , (b) amplitude of time-derivative of normal force coefficient at  $0.87R$  on the retreating side of the rotor  $\left(dC_n M^2/d\psi\right)_{amp}^{ret}$ , (c) amplitude of acoustic pressure signal at the advancing-side microphone  $p_{amp}^{adv}$ , (d) amplitude of acoustic pressure signal at the retreating-side microphone  $p_{amp}^{ret}$ , (e) overall noise levels at the advancing-side microphone  $OASPL^{adv}$  and (f) overall noise levels at the retreating-side microphone  $OASPL^{ret}$ . The microphone positions considered are the ones reported in Ref. 12.

Before commencing the UQ process, the predictive accuracy of the derived PCE is assessed through Leave-One-Out Cross-Validation (LOOCV). The leave-one-out method is based on the construction of a dedicated PCE at each collocation point after excluding this specific point from the dataset. Then, the PCE-predicted value of the objective functions at this sample point is compared with the corresponding value obtained from the direct evaluation of this point using the actual simulation model. The aforementioned process is repeated for the entire set of sample points of the PCE procedure. The quality of the original PCE is assessed in terms of Pearson's product moment of correlation  $N_{Pearson}$  along with the gradient of the associated linear regression line Ref. 40. A perfectly linear correlation would correspond to  $N_{Pearson} = 1.00$  and a regression line gradient of 45.00 deg.

Table 2 summarizes the statistical properties of LOOCV for all objectives corresponding to the case of known experimental data for tip vortex core calibration. Good linear correlation is observed for all objectives, with  $N_{Pearson}$  and gradients very close to the ideal values. This showcases the ability of the developed PCE to replicate the physical behavior of the direct simulation. Furthermore, the normalized root-mean-square error (NRMSE) of each objective is lower than 1.004% which quantified the predictive accuracy of the developed PCE. Finally, the corresponding standard deviation  $\sigma$  of the calculated error is again in the same order for all variables. This indicates that the PCE error is uniformly distributed throughout the investigated design space. As regards the case of absent experimental data with uniformly distributed uncertain inputs with  $COV = 30\%$  (Table 2), similar trends with the previous case are observed, albeit with slightly higher NRMSE (less than 2%), which is attributed to the wider spread of the vortex-core related input variables. However, higher values of output uncertainty are anticipated in this case, which brings the relative contribution of LOOCV uncertainty to similar levels to the  $COV = 10\%$  Gaussian case. Summarizing, the quantification of quality and accuracy of the developed PCE confirms the applicability of the method in the context of uncertainty quantification for BVI noise prediction.

### **Uncertainty quantification**

The derived PCE-based meta-models are utilized for UQ in BVI noise prediction subject to tip vortex core radius uncertainty. The UQ is implemented through MC simulation based on numerical approximations carried out using the PCE meta-model. Table 3 provides the results of UQ for the case when vortex-core experimental data are available (Gaussian distribution with  $COV = 10\%$  ).

It is observed that the standard deviations of  $\left(dC_n M^2/d\psi\right)_{amp}^{adv}$  and  $\left(dC_n M^2/d\psi\right)_{amp}^{ret}$  reach 15.35% and 11.90% of the associated mean values, respectively.

As regards  $p'_{amp}^{adv}$  and  $p'_{amp}^{ret}$ , the non-deterministic mean values are slightly higher than the corresponding deterministic amplitudes (0.36% and 0.88%), with associated uncertainties of 11.78% and 11.93%, respectively. The non-deterministic prediction of mean  $OASPL^{adv}$  and  $OASPL^{ret}$  is almost identical to the corresponding deterministic noise values. The associated uncertainty is 1.02% for both microphone locations, which represents a standard deviation of approximately 1.1 dB.

The skewness  $\gamma_1$  of each objective describes the degree of distortion from the symmetrical “bell-shaped” distribution. It can be seen that for the  $COV=10\%$  case with Gaussian input uncertainty distributions, the non-deterministic output objectives are symmetrical, with values of  $\gamma_1$  generally below 0.5. Especially for  $OASPL^{adv}$  and  $OASPL^{ret}$ , skewness is below 0.05 which corresponds to an almost fully-symmetrical distribution. The excess kurtosis  $\Delta\gamma_2 = \gamma_2 - \gamma_2^{Gaussian}$  is a measure of outliers present in the distribution. It is noted that the kurtosis of Gaussian distribution is  $\gamma_2^{Gaussian} = 3$  by definition. Hence, a value of  $\Delta\gamma_2 = 0$  would represent a perfectly Gaussian distribution. It is shown that for the  $COV=10\%$  case with Gaussian input uncertainty the non-deterministic output objectives follow distributions close to mesokurtic, with values of  $\Delta\gamma_2$  generally below 0.5. Overall, it can be concluded that in cases when experimental data referring to the tip vortex core radius are available, acoustic pressure predictions of less than 12% uncertainty can be made. Similarly, OASPL predictions of less than 1.2dB uncertainty can be made, which confirms the suitability of free-wake/FW-H approaches in the context of complex BVI noise prediction.

Table 3 also presents the uncertainty analysis for the case of absent experimental evidence regarding tip vortex core radius, essentially described by uniformly distributed uncertain input variables with  $COV = 30\%$ . Trends similar to the  $OCV=10\%$  case are observed, albeit with higher levels of uncertainty. Specifically, the uncertainty in  $p'_{amp}{}^{adv}$  and  $p'_{amp}{}^{ret}$  prediction is approximately 25% for both microphone locations, whilst the associated non-deterministic mean values are 3.75% and 12.84% higher than the corresponding deterministic predictions. Standard deviations of 3.71 dB and 3.32 dB are calculated for the  $OASPL^{adv}$  and  $OASPL^{ret}$  objectives, respectively, although these retain non-deterministic mean predictions almost identical to the deterministic ones.

Furthermore, the distributions of  $(dC_n M^2 / d\psi)_{amp}$  and  $p'_{amp}$  are moderately skewed to the right with  $\gamma_1$  reaching positive values of almost 1. In this case, the mean value of output objectives is significantly higher than the mode (Mo) of the distributions, which is the objective value with the highest probability of occurrence. Hence, by neglecting the input uncertainty in this case, the most probable output would be an under-estimated descriptor of unsteady airloads or acoustic pressure. Nevertheless, the symmetry of OASPL is retained at even high values of input uncertainty. However, the associated excess kurtosis is considerably negative, with values lower than  $\Delta\gamma_2 = -0.5$ , which is due to the uniform input distribution.

### Sensitivity analysis

The relative contribution of individual uncertain inputs to the overall response is quantified through sensitivity analysis based on Sobol indices. Table 4 presents the sensitivity indices  $S_i$  referring to the case of available tip-vortex data with Gaussian



$COV = 10\%$  as well as the case of non-available data with uniform  $COV = 30\%$ . It is observed that uncertainty in the parameters used for wake calculations,  $r_{c0}^{wake}$  and  $\alpha_1^{wake}$ , has insignificant influence on all the aeroacoustic outputs. However, inflow-related input uncertainty and especially uncertainty in the value of Squire parameter  $\alpha_1^{inflow}$  has approximately 72% contribution to the overall system's response. It is noted that similar trends have been observed in the sensitivity analysis of the  $COV = 30\%$  case with uniform input distributions, which illustrates that the relative contribution of input parameters is not dependent upon the distribution and range of input uncertainty.

Additionally, it is observed that the sensitivity indices of  $\alpha_1^{inflow}$  are consistently higher at the advancing side, compared with the corresponding indices of retreating side. This is attributed to the tip vortex behavior at both sides of the rotor. As shown in Refs. 9, 10, retreating rotor blades interact with trailed tip vortices of age less than 90 deg. At the early stages of tip vortex propagation, vortex core growth is minimal, which in combination with a small  $r_{c0}$  can lead to small vortex core radii, hence high induced velocities near the core axes and eventually airloads. This highlights the importance of the initial vortex core radius parameter in UQ of retreating-side BVI noise. As regards advancing-side BVIs, most of interactions comprise relatively older tip vortex filaments with an age greater than 90 deg., hence the impact of  $r_{c0}^{inflow}$  is reduced relative to the retreating-side BVI uncertainty. Identical trends are observed for the  $COV=30\%$  case, which illustrates that the system sensitivities are not dependent upon the levels and the shape of the uncertain input distributions.

### **Non-deterministic aeroacoustic predictions**

Fig. 6 (a) presents the non-deterministic prediction of full time-history of a

single BVI acoustic pressure pulse for the case of Gaussian  $COV = 10\%$  input distribution of the tip vortex core parameters. The acoustic pressure time-histories of all sample collocation points have been aligned together to remove any phase shift between the 60 acoustic signals. The illustrated acoustic pressure distribution represents the mean  $p'^{adv}(t)$  value at each point of the time-history. The distribution of non-deterministic mean acoustic pressure is almost identical to the deterministic predictions illustrated in Fig. 4 (a). Superimposed are the uncertainty bars representing two standard deviations of  $p'^{adv}(t)$  at each time-point. It can be seen that a standard deviation of 4.23 Pa corresponds to the positive peak of BVI pulse, whilst a 5.15 Pa standard deviation is calculated at the negative peak. The summary of the aforementioned standard deviations with the amplitude of mean  $p'^{adv}(t)$  results in the non-deterministic amplitude of acoustic pressure. The obtained non-deterministic amplitude of acoustic pressure is very close to the  $p'_{amp}^{adv} = 9.91 \text{ Pa}$  calculated in the “Comparison with experimental measurements” section, which confirms the suitability of the employed descriptor as objective of the UQ process.

Fig. 6 (b) presents the corresponding prediction for uniformly distributed input variables with  $COV = 30\%$ . The mean non-deterministic acoustic pressure distribution is similar to the deterministic, with peak local differences reaching 2.1%. The width of uncertainty bars follows same trends as in the Gaussian  $COV = 10\%$  case, however, the maximum standard deviations reach 14.67 Pa and 15.55 Pa at the positive and negative peaks of the BVI pulse, respectively.

The distribution of uncertainty in the time-domain in the non-deterministic prediction of acoustic pressure is reflected on the frequency range where BVI noise is dominant. Fig. 6 (a) and Fig. 6 (b) illustrate the mean Sound Pressure Levels (SPL)

with superimposed uncertainty bars of  $2\sigma$  corresponding to the  $COV = 10\%$  and  $COV = 30\%$  cases, respectively. The non-deterministic mean values are identical across the entire frequency range, which confirms the immunity of mean SPL to vortex core input uncertainties. For the case of Gaussian input with  $COV = 10\%$ , relatively small levels of uncertainty are observed across the entire frequency range, with standard deviations in the order of 1 dB. This highlights the robustness of free-wake/FW-H approaches in predicting BVI noise when experimental data referring to tip vortex core growth are available. However, in the case without this data, uncertainties in the order of 3.5 dB govern the mid-frequency content, corresponding to the BVI signal, which can primarily be attributed to the high standard deviations observed around the peaks of the acoustic pressure pulse. It is noted that the low-frequency harmonic noise is less affected by vortex-core-related uncertainty, as standard deviations below 1 dB are associated with the first three BPF harmonics.

The impact of uncertainty in the BVI noise predictions is illustrated in Fig. 7 (a) and Fig. 7 (b), which present the distribution of standard deviation in dB for the non-deterministic prediction of 6-40 BPF mean noise distribution of the HART II experiment (Ref. 12). It is noted that the mean OASPL distribution is very similar to the deterministic equivalent presented in Fig. 5 (b), hence it was deemed sufficient to only present the corresponding standard deviations. Generally, the prediction of noise contour maps is adequately robust in the  $COV = 10\%$  case, with values of standard deviations not exceeding 1 dB at most measurement nodes. As regards the uniform-input  $COV = 30\%$  case, uncertainty can reach up to 4.6 dB, which highlights the importance of non-deterministic simulation when experimental evidence referring to the vortex core geometry is not available.

### Fundamental modeling guidelines

The previous analysis has shown that the impact of input uncertainty on the robustness of aeroacoustic predictions is dependent upon the shape and COV of input distributions. Fig. 8 (a) and Fig. 8 (b) present the probability histograms of  $p'_{amp}{}^{adv}$ , comparing the cases of Gaussian and uniform uncertain input distributions, for  $COV=10\%$  and  $COV=30\%$ , respectively. The distributions are expressed as relative deviation from the  $p'_{amp}{}^{adv}$  which achieves the best match with experimental data, as presented in Fig. 4 (a). This value will be used as reference for the analysis presented in this section. The percentage deviation of the mode of the distribution relative to the reference is defined as  $\Delta(Mo|ref)\% = \frac{Mo_{(.)} - ref_{(.)}}{ref_{(.)}} 100\%$ . Similarly, the

percentage deviation of the mean value of  $p'_{amp}{}^{adv}$  from the reference is defined as

$$\Delta(\mu|ref)\% = \frac{\mu_{(.)} - ref_{(.)}}{ref_{(.)}} 100\%.$$

For the  $COV=30\%$  case, it can be seen that both

distributions are positively skewed resulting in modes with  $\Delta(Mo|Ref) = -25\%$  from the reference. This depicts the importance of non-deterministic simulation at high values of input uncertainty: a 25% under-prediction of  $p'_{amp}{}^{adv}$  is the event with highest probability if the parameters of the tip vortex core growth model are randomly defined within the given bounds. On the other hand, non-deterministic simulation results in only  $\Delta(\mu|ref)\% = 5.8\%$  over-prediction of the mean value of  $p'_{amp}{}^{adv}$  relative to the explicit reference.

The uncertainty quantification method described in the “Mathematical formulation” section is repeated for a wide range of input COV and for two different shapes of input distributions, Gaussian and uniform. The outcome of this process is a

set of generalized uncertainty maps which can serve as modeling guidelines in the aeroacoustic analysis of civil rotorcraft. Fig. 9 (a) illustrates the uncertainty map referring to  $p_{amp}^{adv}$  and  $OASPL^{adv}$  for input COV ranging from 0% to 55% for Gaussian input distribution. Fig. 9 (b) presents the corresponding results for both objectives for the case of uniform input distributions. Each point of the map essentially represents the outputs of full UQ based on dedicated PCEs comprising 60 collocation points each. Therefore, a total of 1,320 deterministic evaluations were carried out, including free-wake, aeroelastic and aeroacoustic analyses, in order to obtain the results required to arrive towards generic modelling guidelines based on the relative impact of uncertainty in the modelling of tip-vortex core parameters.

The output mean values of  $p_{amp}^{adv}$  predictions are provided as percentage changes relative to the reference, whilst output uncertainty  $\sigma|_{ref}\% = \frac{\sigma(\cdot)}{ref(\cdot)}100\%$  is presented as percentage of the reference. It can be seen that output uncertainty is almost linearly correlated with input uncertainty, with a gradient of approximately 58 deg. for both distributions. As regards the relative deviation of non-deterministic mean  $p_{amp}^{adv}$ , it is described by a 2<sup>nd</sup> order polynomial trend, with values generally higher than the reference. For the uniformly distributed input case,  $\Delta(Mo|_{ref})\%$  presents a diverging trend, leading to under-predictions between 9.3% and 72.2% for input COV greater than 15%. This is the point where input uncertainty starts to become important for the accuracy of acoustic pressure predictions. The difference between the  $\Delta(\mu|_{ref})\%$  and  $\Delta(Mo|_{ref})\%$  curves quantifies the benefits that arise from non-deterministic simulation relative to the outcome with highest probability from the corresponding deterministic execution.

As regards  $OASPL^{adv}$ , absolute non-deterministic metrics are defined in this case. Specifically,  $\Delta(Mo|ref) \text{ dB} = Mo_{(\cdot)} - ref_{(\cdot)}$ ,  $\Delta(\mu|ref) \text{ dB} = \mu_{(\cdot)} - ref_{(\cdot)}$  and  $\sigma|ref \text{ dB} = \sigma_{(\cdot)} - ref_{(\cdot)}$ , all expressed in dB. Generally low  $\Delta(\mu|ref) \text{ dB}$  are observed, with values not exceeding 1 dB even at high levels of input uncertainty. The associated output uncertainty is again linearly correlated with input COV, with a gradient of 6.4 deg.  $\Delta(Mo|ref) \text{ dB}$  presents again a diverging trend, with under-predictions of up to 2 dB at excessively high values of input uncertainty.

Summarizing, for given requirements in terms of accuracy and robustness, the analyst can resort to the developed uncertainty maps in order to: (a) estimate the anticipated error of deterministic simulation (b) evaluate the necessity of non-deterministic simulation and assess the expected improvement in accuracy, and (c) quantify the associated uncertainty depending on output objectives and analysis requirements. The above guidelines are applicable for both detailed acoustic pressure prediction and holistic noise contour map evaluation referring to helicopter rotors in BVI-dominated flight conditions.

It is noted that the impact of PIV measurement techniques and post-processing methods affect the magnitude of input uncertainty used for the non-deterministic simulation. Therefore, this work can be extended through investigating the sensitivity of output uncertainty quantification to different tip vortex characterization techniques.

The results of this study can be further expanded towards a holistic uncertainty quantification campaign, including all major sources of aleatoric and epistemic uncertainty that affect the prediction of helicopter noise.

## Conclusions

A holistic analysis was undertaken, examining the impact of tip vortex core growth modeling uncertainty on the robustness of aeroacoustic simulation of helicopter rotors in BVI conditions. A coupled approach using free-wake aerodynamic and Ffowcs Williams-Hawkings aeroacoustic models was employed. Two distinct cases were defined for uncertainty analysis: (a) when experimental data about the geometry of tip vortex core are available and (b) when experimental data are absent. For both cases uncertainty quantification was conducted based on Polynomial Chaos expansion. A sensitivity analysis based on Sobol indices was carried out to identify the relative contribution of each uncertain parameter to the overall non-deterministic response of the system. The output objectives for statistical analysis were descriptors representative of unsteady rotor airloads, acoustic pressure and OASPL noise.

It was shown that in the case of availability of experimental data, the levels of OASPL uncertainty are in the order of 1 dB, which dictates the suitability of free-wake/FW-H approaches as robust tools for modeling helicopter BVI noise. When vortex-core-related experimental data are absent, output uncertainty in the order of 3.5 dB can occur for conservative selection of input uncertainty. This highlights the necessity of non-deterministic simulation when correlations with tip-vortex experimental data are not feasible.

Furthermore, it was demonstrated that in the absence of experimental evidence, deterministic approaches could lead to acoustic pressure under-predictions in the order of -25%. For the same case, employment of non-deterministic simulation improves the accuracy of simulation to values corresponding to only 5.8% over-predictions, relative to the validated reference acoustic pressure.

A generalized set of non-deterministically derived aeroacoustic predictions

which achieves the best match with experimental data was derived. The simulations were carried out at different levels and distributions of input uncertainty, thus providing an uncertainty map which can serve as modeling guidelines for analysts. Specifically, for given requirements in terms of predictive robustness, the analyst can estimate the anticipated error of their deterministic simulation, evaluate the necessity and benefit of non-deterministic simulation, and quantify the associated levels of uncertainty depending on output objectives and analysis requirements.

### **Acknowledgements**

This work has received funding from the Clean Sky 2 Joint Undertaking under the European Union’s Horizon 2020 research and innovation programme under grant agreement No. 776900. The authors would also like to acknowledge Mr. Jos Stevens (NLR), Dr. Gianluigi Alberto Misté (University of Padua), Mr. Nico van Oosten (Anotec Engineering SL) and Mr. Alf Junior (DLR) for their insightful advice on rotorcraft modeling and simulation.

### **References**

- 1 M. E. Kelly and R. E. Brown, “The effect of blade aerodynamic modelling on the prediction of the blade airloads and the acoustic signature of the HART II rotor,” 2009.
- 2 M. Gennaretti, G. Bernardini, J. Serafini, and G. Romani, “Rotorcraft comprehensive code assessment for blade – vortex interaction conditions,” *Aerospace Science and Technology*, vol. 80, pp. 232–246, 2018, doi: 10.1016/j.ast.2018.07.013.
- 3 B. Giret, S. Moreau, and J. Boussuge, “Uncertainty quantification of the far-field noise from a rod-airfoil configuration,” in *Proceedings of the Summer Program, Center for Turbulence Research, Stanford University, NASA*, 2012,



- pp. 261–270.
- 4 B. Ivo, F. Nobile, and R. Tempone, “A stochastic collocation method for elliptic partial differential equations with random input data,” *SIAM Journal on Numerical Analysis*, vol. 45, no. 3, pp. 1005–1034, 2007.
  - 5 W. F. J. Olsman, “Uncertainty quantification of noise abatement flight procedures,” in *41st European Rotorcraft Forum Proceedings*, 2015, p. 32.
  - 6 N. Ricks, S. Abraham, F. Contino, and G. Ghorbaniasl, “Sensitivity Analysis and Uncertainty Quantification for the Ffowcs Williams-Hawkins Equation,” in *23rd AIAA/CEAS Aeroacoustics Conference*, 2017, p. 3511, doi: 10.2514/6.2017-3511.
  - 7 N. Ricks, S. Abraham, F. Contino, and G. Ghorbaniasl, “Uncertainty quantification for the aeroacoustics of rotating blades in the time domain,” *Applied Acoustics*, vol. 139, no. April, pp. 57–68, 2018, doi: 10.1016/j.apacoust.2018.04.012.
  - 8 M. J. Bhagwat and M. Ramasamy, “Effect of tip vortex aperiodicity on measurement uncertainty,” *Experiments in fluids*, vol. 53, no. 5, pp. 1191–1202, 2012, doi: 10.1007/s00348-012-1348-7.
  - 9 S. M. Mula and C. E. Tinney, “A study of the turbulence within a spiralling vortex filament using proper orthogonal decomposition,” *Journal of Fluid Mechanics*, vol. 769, no. January 2016, pp. 570–589, 2015, doi: 10.1017/jfm.2015.104.
  - 10 B. G. Van Der Wall and H. Richard, “Analysis methodology for 3C-PIV data of rotary wing vortices,” *Experiments in Fluids*, vol. 40, no. 5, pp. 798–812, 2006, doi: 10.1007/s00348-006-0117-x.
  - 11 S. M. Mula, J. H. Stephenson, C. E. Tinney, and J. Sirohi, “Dynamical characteristics of the tip vortex from a four-bladed rotor in hover,” *Experiments in Fluids*, vol. 54, no. 10, 2013, doi: 10.1007/s00348-013-1600-9.
  - 12 B. G. van der Wall, J. W. Lim, J. D. Baeder, and D. D. Boyd, “The HART II international workshop: an assessment of the state-of-the-art in comprehensive code prediction,” *CEAS Aeronautical Journal*, vol. 4, no. 3, pp. 223–252, 2013, doi: 10.1007/s13272-013-0077-9.
  - 13 A. Castillo Pardo, “Aeroelastic Simulation of Rotorcraft Propulsion Systems,” *Ph.D. thesis, Cranfield University, Cranfield, Bedfordshire, UK*, 2017.
  - 14 I. Goulos, V. Pachidis, and P. Pilidis, “Lagrangian Formulation for the Rapid

- Estimation of Helicopter Rotor Blade Vibration Characteristics,” *The Aeronautical Journal*, vol. 118, no. 1206, pp. 861–901, 2014, doi: 10.1017/S000192400000960X.
- 15 A. Castillo Pardo, I. Goulos, and V. Pachidis, “Modelling and analysis of coupled flap-lag-torsion vibration characteristics helicopter rotor blades,” *Proceedings of the Institution of Mechanical Engineers, Part G: Journal of Aerospace Engineering*, vol. 231, no. 10, pp. 1804–1823, 2016, doi: 10.1177/0954410016675891.
- 16 I. Goulos, V. Pachidis, and P. Pilidis, “Helicopter Rotor Blade Flexibility Simulation for Aeroelasticity and Flight Dynamics Applications,” *Journal of the American Helicopter Society*, vol. 59, no. 4, pp. 1–18, 2014, doi: 10.4050/JAHS.59.042006.
- 17 J. G. Leishman and T. S. Beddoes, “A Semi-Empirical Model for Dynamic Stall,” *Journal of the American Helicopter Society*, vol. 3, pp. 3–17, 1989.
- 18 A. Bagai and J. G. Leishman, “Rotor Free-Wake Modeling Using a Pseudo-Implicit Technique — Including Comparisons with Experimental Data,” *Journal of the American Helicopter Society*, vol. 40, no. 3, pp. 29–41, 1995, doi: 10.4050/JAHS.40.29.
- 19 H. Chen, K. S. Brentner, S. Ananthan, and J. G. Leishman, “A Computational Study of Helicopter Rotor Wakes and Noise Generated During Transient Maneuvers,” *Journal of the American Helicopter Society*, vol. 53, no. 1, pp. 37–55, 2008, doi: 10.4050/JAHS.53.37.
- 20 G. H. Vatistas, V. Kozel, and W. C. Mih, “A simpler model for concentrated vortices,” *Experiments in Fluids*, vol. 11, no. 1, pp. 73–76, 1991, doi: 10.1007/BF00198434.
- 21 M. J. Bhagwat and J. G. Leishman, “Generalized viscous vortex model for application to free-vortex wake and aeroacoustic calculations,” 2002.
- 22 S. Vouros, I. Goulos, and V. Pachidis, “Integrated methodology for the prediction of helicopter rotor noise at mission level,” *Aerospace Science and Technology*, vol. 89, pp. 136–149, 2019, doi: 10.1016/j.ast.2019.03.061.
- 23 S. Vouros, “Aeroacoustic Simulation of Rotorcraft Propulsion Systems,” *PhD Thesis, Cranfield University*, 2019.
- 24 J. E. Ffowcs Williams and D. L. Hawkings, “Sound Generation by Turbulence and Surfaces in Arbitrary Motion,” *Philosophical Transactions of the Royal*

- Society of London. Series A, Mathematical and Physical Sciences*, vol. 264, no. 1151, pp. 321–342, 1969, doi: 10.1098/rsta.1969.0031.
- 25 M. J. Lighthill, “On Sound Generated Aerodynamically. I. General Theory,” *Proceedings of the Royal Society A: Mathematical, Physical and Engineering Sciences*, vol. 211, no. 1107, pp. 564–587, 1952, doi: 10.1098/rspa.1952.0060.
  - 26 F. Farassat, “Derivation of Formulations 1 and 1A of Farassat,” *NASA/TM-214853*, 2007.
  - 27 F. Farassat and G. P. Succi, “The prediction of helicopter rotor discrete frequency noise,” 1982.
  - 28 K. S. Brentner, C. L. Burley, and M. A. Marcolini, “Sensitivity of Acoustic Predictions to Variation of Input Parameters,” *Journal of the American Helicopter Society*, vol. 39, no. 3, pp. 43–52, 1994.
  - 29 L. V. Lopes, “Compact Assumption Applied to the Monopole Term of Farassat’s Formulations,” *21st AIAA/CEAS Aeroacoustics Conference, AIAA 2015-2673*, pp. 1–22, 2015.
  - 30 S. Lee, K. S. Brentner, F. Farassat, and P. J. Morris, “Analytic Formulation and Numerical Implementation of an Acoustic Pressure Gradient Prediction,” *Journal of Sound and Vibration*, vol. 319, no. 3–5, pp. 1200–1221, 2009, doi: 10.1016/j.jsv.2008.06.028.
  - 31 L. V. Lopes, “Compact Assumption Applied to Monopole Term of Farassat’s Formulations,” *Journal of Aircraft*, vol. 54, no. 5, pp. 1649–1663, 2017, doi: 10.2514/1.C034048.
  - 32 S. Murugan, R. Ganguli, and D. Harursampath, “Stochastic aeroelastic analysis of composite helicopter rotor,” *Journal of the American helicopter society*, vol. 56, no. 1, p. 12001, 2011, doi: 10.4050/JAHS.56.012001.
  - 33 C. Siva, S. Murugan, and G. Ganguli, “Uncertainty quantification in helicopter performance using Monte Carlo simulations,” *Journal of Aircraft*, vol. 48, no. 5, pp. 1503–1511, 2011, doi: 10.2514/1.C000288.
  - 34 D. Xiu and G. E. M. Karniadakis, “The Wiener--Askey polynomial chaos for stochastic differential equations,” *SIAM journal on scientific computing*, vol. 24, no. 2, pp. 619–644, 2002.
  - 35 S. Hosder, R. Walters, and M. Balch, “Efficient Sampling for Non-Intrusive Polynomial Chaos Applications with Multiple Uncertain Input Variables,” in *48th AIAA/ASME/ASCE/AHS/ASC Structures, Structural Dynamics, and*

- Materials Conference*, 2007, p. 1939.
- 36 M. Berveiller, B. Sudret, and M. Lemaire, “Stochastic finite element: a non intrusive approach by regression,” *European Journal of Computational Mechanics/Revue Européenne de Mécanique Numérique*, vol. 15, no. 1–3, pp. 81–92, 2006.
- 37 I. M. Sobol, “Sensitivity Estimates for Nonlinear Mathematical Models,” *Mathematical modelling and computational experiments*, vol. 1, no. 4, pp. 407–414, 1993.
- 38 H. Toshiimitsu and A. Saltelli, “Importance measures in global sensitivity analysis of nonlinear models,” *Reliability Engineering & System Safety*, vol. 52, no. 1, pp. 1–17, 1996.
- 39 P. J. Roache, “Perspective: A method for uniform reporting of grid refinement studies,” *Journal of Fluids Engineering, Transactions of the ASME*, vol. 116, no. 3, pp. 405–413, 1994, doi: 10.1115/1.2910291.
- 40 I. Goulos and M. Bonesso, “Variable rotor speed and active blade twist for civil rotorcraft: Optimum scheduling, mission analysis, and environmental impact,” *Aerospace Science and Technology*, vol. 1, pp. 1–13, 2019, doi: 10.1016/j.ast.2019.03.040.

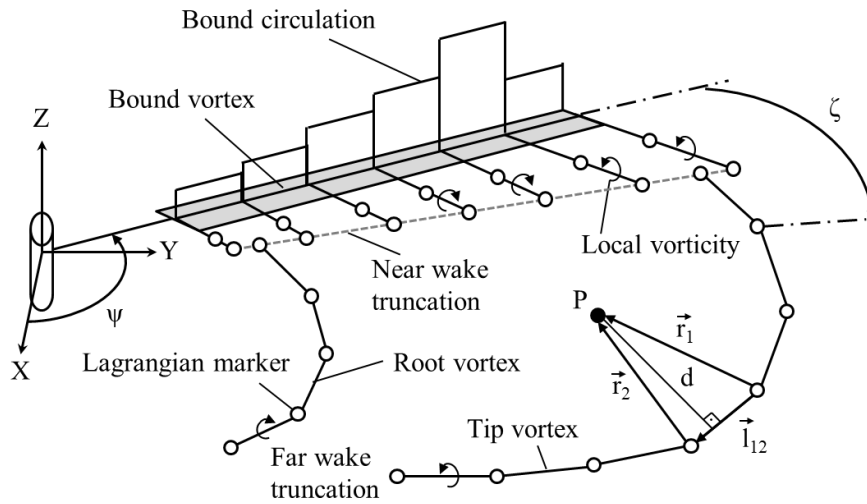


**Fig. 1.** Overview of free-wake aerodynamic model.

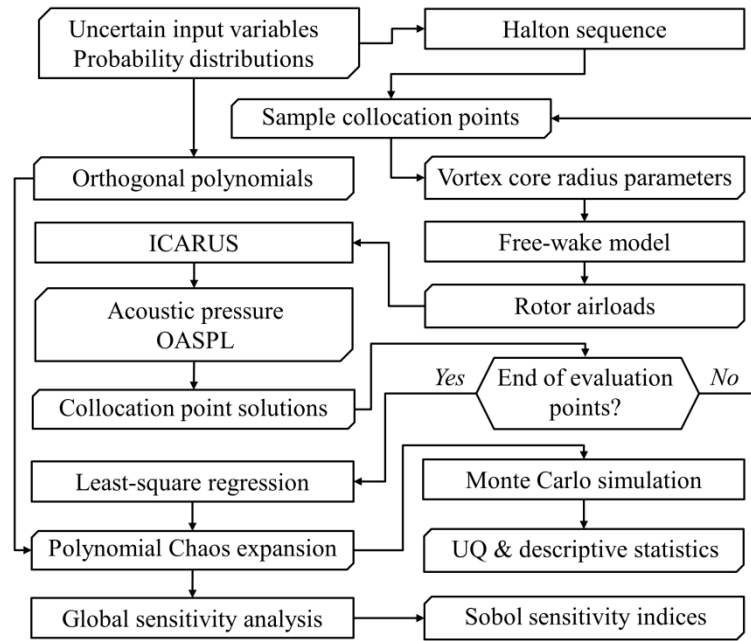


**Fig. 2.** Uncertainty quantification methodology.

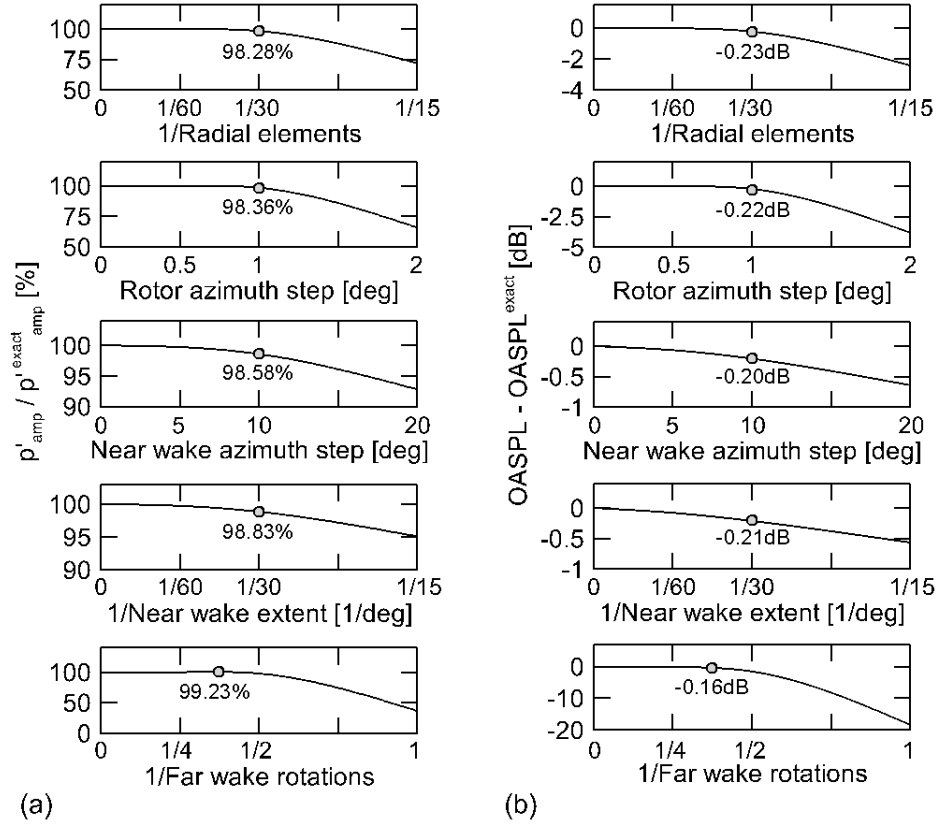


**Fig. 3:** Grid convergence sensitivity analysis and quantification of actual fractional error as function of discretization parameters: (a) evaluation for  $p'_{amp}$  and (b) evaluation for  $OASPL$ .

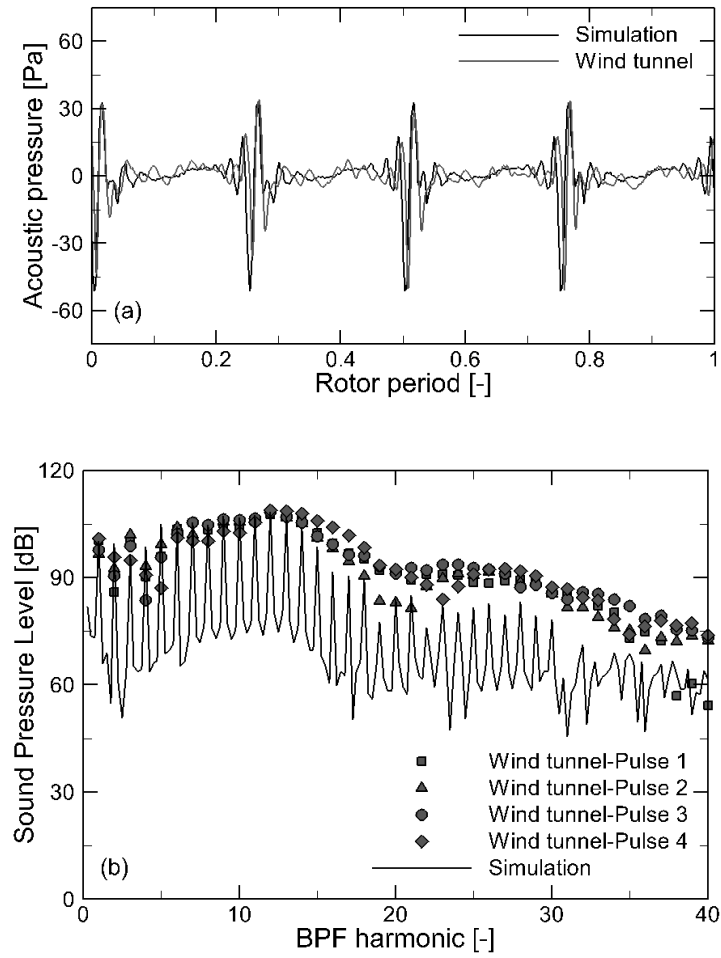


**Fig. 4.** Acoustic pressure prediction for the advancing-side observer of the HART II experiment – comparison with experimental data from Ref. 9: (a) acoustic pressure; (b) spectral analysis.



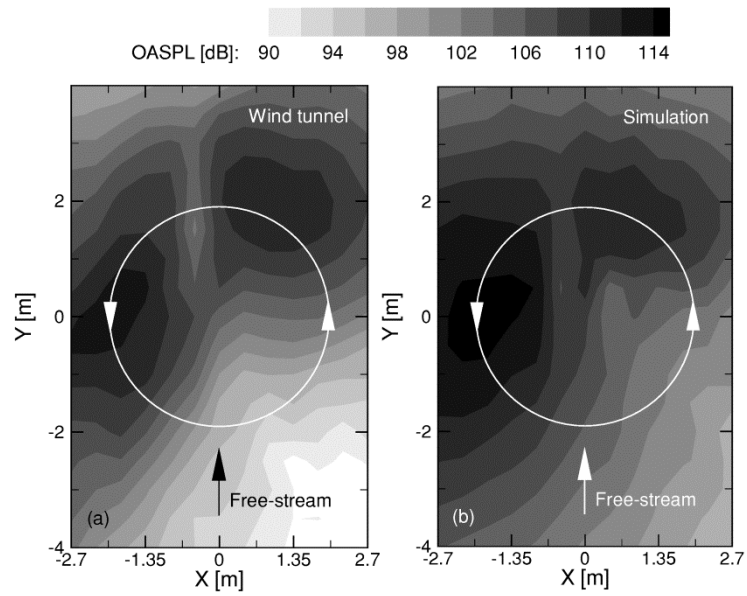


**Fig. 5.** BVI noise contour map prediction between the 6<sup>th</sup> and the 40<sup>th</sup> harmonic 2.215m below the HART II rotor – comparison with experimental data from Ref. 9: (a) wind tunnel; (b) simulation.

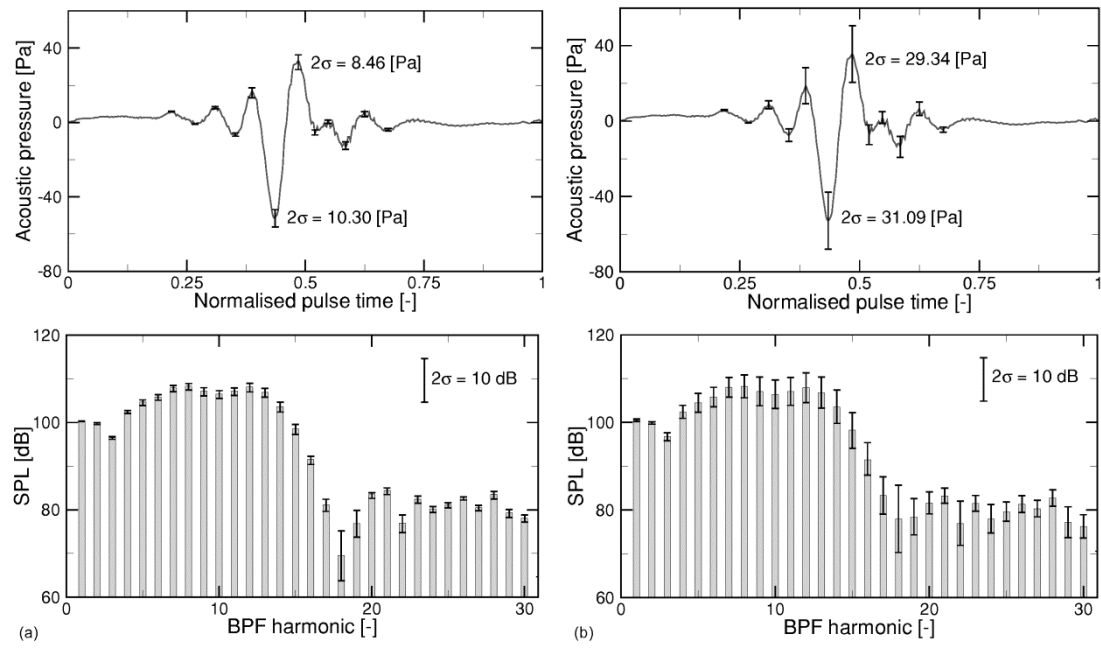


**Fig. 6.** Non-deterministic prediction of acoustic pressure and corresponding spectral content: (a) Gaussian input with COV=10%; (b) Uniform input with COV=30%.

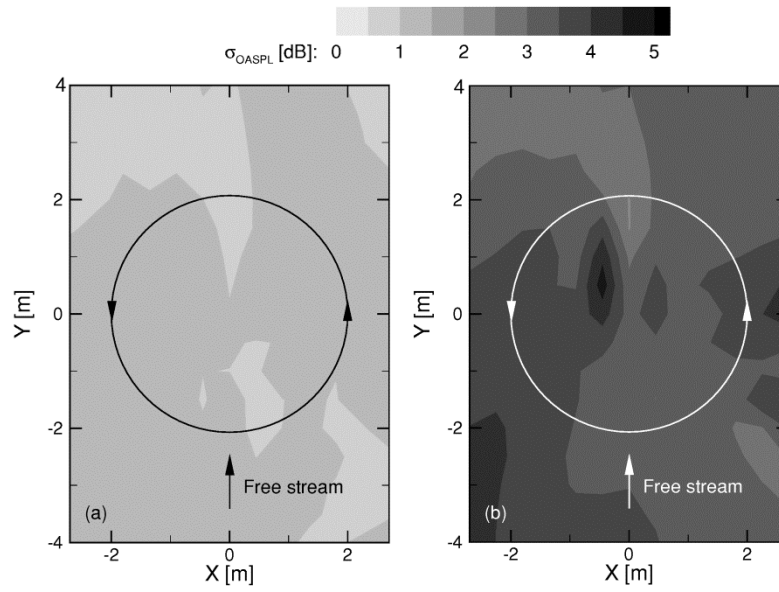


**Fig. 7.** Distribution of standard deviation in noise contour map prediction 2.215m below the HART II rotor: (a) Gaussian input with COV=10%; (b) Uniform input with COV=30%.

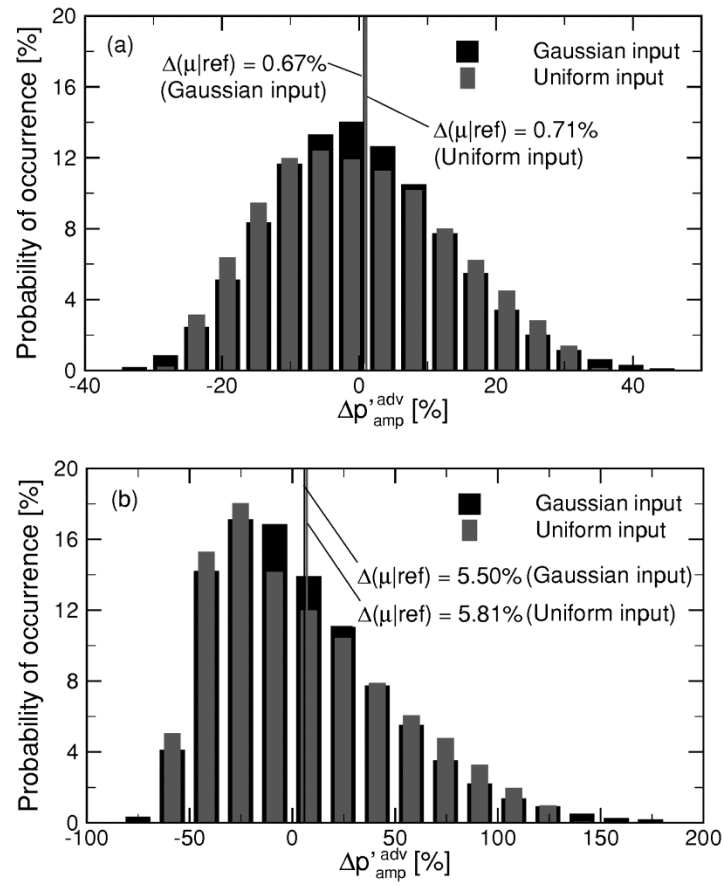


**Fig. 8.** Probability histograms for the deviation of advancing-side acoustic pressure amplitude from the reference value: (a) Input COV=10%; (b) Input COV=30%.

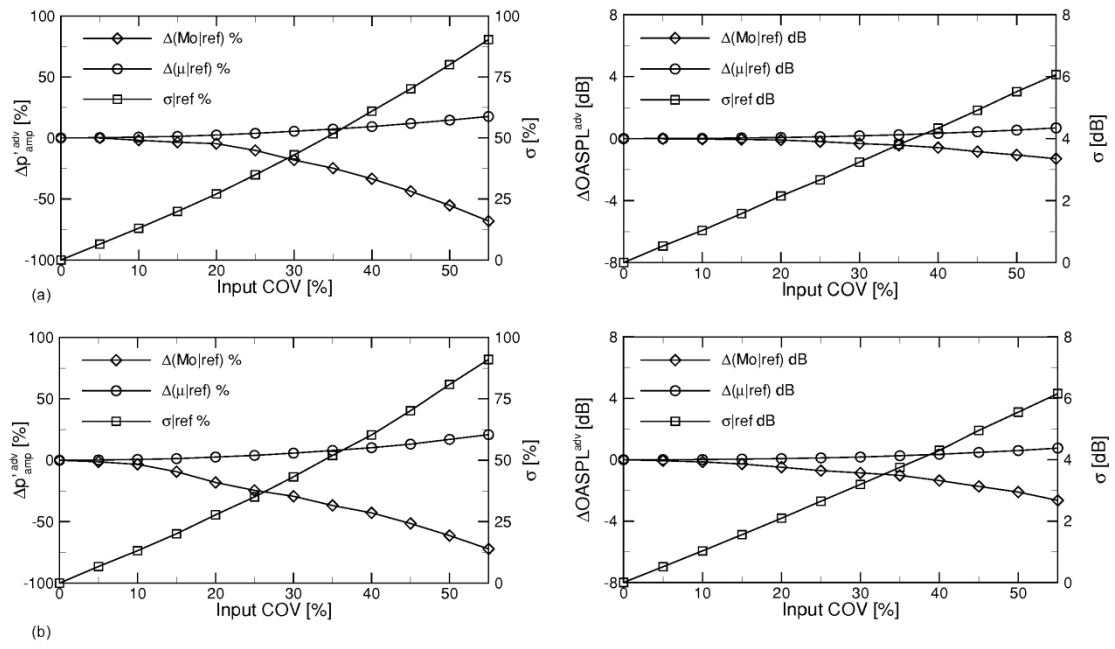


**Fig. 9.** Impact of input uncertainty on the prediction of acoustic pressure and OASPL:

(a) Gaussian input; (b) Uniform input.

**Table 1.** Description of uncertain input variables for the cases of available (Gaussian distribution with COV=10%) and not available (Uniform distribution with COV=30%) tip-vortex growth experimental data.

Uncertain input	Unit	Gaussian (COV=10%)		Uniform (COV=30%)	
		$\mu$	$\sigma$	Min. value	Max. value
$r_{c0}^{wake}$	[chords]	0.10	0.01	0.0480	0.1519
$\alpha_1^{wake}$	[-]	0.001	0.0001	0.00048	0.00152
$r_{c0}^{inflow}$	[chords]	0.60	0.06	0.2882	0.9117
$\alpha_1^{inflow}$	[-]	0.008	0.0008	0.00384	0.01215

**Table 2.** Statistics of LOOCV of the derived PCE for the cases of available (Gaussian distribution with COV=10%) and not available (Uniform distribution with COV=30%) tip-vortex growth experimental data.

Objective	Gaussian (COV=10%)				Uniform (COV=30%)			
	N <sub>Pearson</sub> [-]	Grad. [deg]	NRMSE [%]	$\sigma$ [%]	N <sub>Pearson</sub> [-]	Grad. [deg]	NRMSE [%]	$\sigma$ [%]
$(dC_n M^2 / d\psi)_{amp}^{adv}$	0.999	45.05	0.46	0.47	0.999	45.26	1.82	1.82
$(dC_n M^2 / d\psi)_{amp}^{ret}$	0.995	44.55	1.00	1.01	0.998	45.12	1.96	1.95
$p'_{amp}^{adv}$	0.998	44.68	0.64	0.63	0.999	45.23	1.70	1.71
$p'_{amp}^{ret}$	0.996	45.33	0.97	0.96	0.998	45.19	1.88	1.89
$OASPL^{adv}$	0.999	45.00	0.10	0.11	0.999	44.90	0.19	0.19
$OASPL^{ret}$	0.996	44.76	0.16	0.16	0.998	44.94	0.23	0.23

**Table 3.** Uncertainty quantification for the cases of available (Gaussian distribution with COV=10%) and not available (Uniform distribution with COV=30%) tip-vortex growth experimental data.

Objective [unit]	Gaussian (COV=10%)				Uniform (COV=30%)			
	$\mu$ [unit]	$\sigma$ [unit]	$\gamma_1$ [-]	$\Delta\gamma_2$ [-]	$\mu$ [unit]	$\sigma$ [unit]	$\gamma_1$ [-]	$\Delta\gamma_2$ [-]
$(dC_n M^2 / d\psi)_{amp}^{adv} [rad^{-1}]$	0.82	0.12	0.422	0.112	0.87	0.28	0.946	-0.037
$(dC_n M^2 / d\psi)_{amp}^{ret} [rad^{-1}]$	0.62	0.07	0.608	0.364	0.67	0.18	0.841	-0.008
$p'_{amp}^{adv} [Pa]$	84.12	9.91	0.327	0.046	86.96	21.74	0.704	-0.267
$p'_{amp}^{ret} [Pa]$	46.64	5.56	0.318	0.024	48.37	12.43	0.782	-0.074
$OASPL^{adv} [dB]$	114.4	1.17	0.013	-0.113	114.61	3.71	0.024	-0.705
$OASPL^{ret} [dB]$	111.1	1.14	0.027	-0.064	111.21	3.32	0.061	-0.618



**Table 4.** Sensitivity analysis for the cases of available (Gaussian distribution with COV=10%) and not available (Uniform distribution with COV=30%) tip-vortex growth experimental data.

Objective	Sensitivity index $S_i$ [%]							
	Gaussian (COV=10%)				Uniform (COV=30%)			
	$r_{c0}^{wake}$	$\alpha_1^{wake}$	$r_{c0}^{inflow}$	$\alpha_1^{inflow}$	$r_{c0}^{wake}$	$\alpha_1^{wake}$	$r_{c0}^{inflow}$	$\alpha_1^{inflow}$
$(dC_n M^2 / d\psi)_{amp}^{adv}$	0.01	0.01	27.61	72.36	0.04	0.05	29.65	70.25
$(dC_n M^2 / d\psi)_{amp}^{ret}$	0.02	0.02	35.51	64.19	0.02	0.10	36.72	62.91
$p'_{amp}^{adv}$	0.01	0.01	27.38	72.59	0.02	0.03	28.37	71.57
$p'_{amp}^{ret}$	0.03	0.01	46.92	53.03	0.13	0.04	40.23	59.59
$OASPL^{adv}$	0.01	0.01	27.75	72.22	0.01	0.02	28.86	71.11
$OASPL^{ret}$	0.02	0.01	47.17	52.80	0.04	0.01	40.19	59.76

2020-09-04

# Impact of tip-vortex modeling uncertainty on helicopter rotor blade-vortex interaction noise prediction

Vouros, Stavros

Vertical Flight Society

---

Vouros S, Goulos I, Scullion C, Nalianda D, et al., (2020) mpact of tip-vortex modeling uncertainty on helicopter rotor blade-vortex interaction noise prediction. Journal of the American Helicopter Society, Volume 66, number 1, January 2021, pp. 1-13

<https://doi.org/10.4050/JAHS.66.012005>

*Downloaded from Cranfield Library Services E-Repository*